Journal of Photochemistry and Photobiology A: Chemistry 203 (2009) 24–31

Contents lists available at ScienceDirect

Journal of Photochemistry and Photobiology A: Chemistry

journal homepage: www.elsevier.com/locate/jphotochem

Physico-chemical, photo-catalytic and O_2-adsorption properties of TiO_2 nanotubes coated with gold nanoparticles

Sachin S. Malwadkar, Ramakrishna S. Gholap, Shobhana V. Awate, Prakash V. Korake[1], Manohar G. Chaskar[1], Narendra M. Gupta*

Catalysis Division, National Chemical Laboratory, Dr. Homi Bhabha Road, Pune 411008, India

ARTICLE INFO

Article history:
Received 22 July 2008
Received in revised form 23 October 2008
Accepted 9 December 2008
Available online 24 December 2008

Keywords:
TiO_2 nanotubes
Gold co-catalyst
Photo-catalytic activity
O_2-adsorption
Acetaldehyde oxidation

ABSTRACT

Gold-containing titania nanotubes (Au/NT) were found to display higher activity for photooxidation of acetaldehyde, as compared to corresponding gold-free nanotubes and also a Degussa P-25 catalyst. Besides CO_2 as a major reaction product, small amounts of H_2, CH_4, CO, H_2O and CH_3COOH were also formed, irrespective of the catalyst employed. High-resolution TEM examination showed that most of the gold particles in Au/NT were of 1.5–5 nm size, distributed both within and at outside surface of the nanotubes. Some larger size (10–70 nm) clusters were also seen at the external surfaces, particularly in the samples calcined at an elevated temperature. The temperature-programmed desorption measurements revealed that, compared to P-25 TiO_2, a significant entrapment of O_2 occurred at two distinct tubular sites of NT samples, corresponding activation energy of desorption (E_a) being around 36 and 41 kcal mol^{-1}. On the other hand, gold nanoparticles in Au/NT served as independent low-energy (E_a = 26 kcal mol^{-1}) sites for adsorption/activation of O_2. These adsorptive properties of TiO_2 and Au were lost completely on calcination, thus revealing a crucial role played by the particle size. *In situ* IR spectroscopy results showed that room-temperature exposure to acetaldehyde + air gave rise to a molecularly bound state, i.e. CH_3CHO_{ad}, over both NT and Au/NT samples, which in turn transformed quickly to yield certain acetate ($CH_3COO^-{}_{ad}$) and formate ($HCOO^-{}_{ad}$) type transient species with the involvement of the surface OH groups. The decomposition and oxidation of these surface species with the help of O_2^-, O_{ad} and hydroxyl ion radicals (OH^-) formed at photo-excited Au/NT interfaces led to the reaction products mentioned above. We conclude that, besides electron–hole charge separation, the adsorptive properties of host matrix and nanosize gold may together play a significant role in deciding the photo-catalytic properties of Au/TiO_2.

1. Introduction

The photophysical and photo-catalytic properties of nanoscale semiconductor particles are known to be considerably influenced by the so-called quantum-(Q-) size related band gap changes. As reviewed in several articles [1–4], use of size-quantized semiconductor TiO_2 particles is found to increase the photo-efficiency for those systems in which the rate limiting step involves a charge transfer. In certain other reaction systems, a decrease in photoactivity is reported where surface speciation and surface defect density may play an important role. In addition, doping of TiO_2 by various metal ions is shown to further enhance the quantum yield in a large number of photooxidation and reduction reactions [5]. Discrepant views have, however, been expressed in regards to the influence of these chemical and morphological modifications in TiO_2 on the primary steps involved in photo-catalytic processes. As per one school of thought, the textural properties of TiO_2 may affect the charge carrier relaxation dynamics. For instance, Serpone et al. [6] proposed that the dominant e^-/h^+ recombination pathway may be different for TiO_2 samples of different particle size regimes. Zhang et al. [7] reported that nanosize ($\leq$11 nm diameter) crystallites of TiO_2 exhibit improved photonic efficiency by inhibiting the surface e^-/h^+ recombination process. It is also reported that a smaller size of semiconductor particles leads to the enhanced redox potential of valence band holes and conduction electrons [8]. Similarly, while reviewing the chemistry of semiconductor nanoparticles, Khairutdinov [9] has highlighted the effect of particle size on redox properties and the spatial separation of electrons and holes in such structures. In another study concerning semiconductor-metal nano-structures, the improved photoelectrochemical performance is attributed to the shift in quasi-Fermi level of the composite to more negative potentials [10]. Wu et al. [11] showed that while the crystalline nature was important for the photo-catalytic activity of TiO_2 based catalysts, the function of doped transition metal was to increase the electron–hole recombination time. On the other

* Corresponding author. Tel.: +91 20 25902008; fax: +91 20 25902633.
E-mail address: nm.gupta@ncl.res.in (N.M. Gupta).
[1] Waghire College, Saswad, Pune, India.

1010-6030/$ – see front matter © 2008 Elsevier B.V. All rights reserved.
doi:10.1016/j.jphotochem.2008.12.013

Table 1
Physical properties of TiO_2 and Au/TiO_2 photo-catalysts.

Details of TiO_2 sample	Notation	Calcination temperature, K	Surface area, $m^2\ g^{-1}$	Crystallite size, nm	Average pore dimension, nm
Degussa P-25	T1	–	59.0	20.0	–
Nanotubes	NT1	423	180.0	6.3	5.6
Nanotubes	NT2	523	145.2	7.8	6.0
1% wt. Au over NT1	Au(1%)/NT1	423	163.4	5.0	–
1% wt. Au over NT2	Au(1%)/NT2	523	115.2	6.5	5.5
1.5 wt.% Au over NT2	Au(1.5%)/NT2	523	76.5	–	4.5

hand, the photo-catalytic activity of mesoporous titania films for degradation of methylene blue is shown to be related to certain surface and morphological properties, such as surface area, pore size distribution and pore accessibility [12]. Also, the activity of silica-supported TiO_2 is found to be influenced by the surface properties of the support [13].

In a recent study, we reported that the enhanced photo-catalytic activity of gold particles dispersed in a meso-structured TiO_2 sample is in fact related directly to the individual adsorptive properties of the host matrix and the Au co-catalyst [14]. Similarly, the visible light mediated catalytic activity of highly dispersed CdS nanocrystals for splitting of water is shown to be structure sensitive [15]. In continuation, we have now conducted detailed investigations on titania nanotubes (denoted as NT for brevity) containing highly dispersed gold particles. The objective was to explore a relationship between the crystallite morphology, both TiO_2 as well as dispersed co-catalyst, and the photo-catalytic properties. We visualized that in addition to higher surface area the tubular design of titania may facilitate the adsorption of the reactant molecules and their transport through the porous network. In order to validate these ideas, the structural and textural properties of Au/NT samples have been examined carefully by using high-resolution transmission electron microscopy (HRTEM), powder X-ray diffraction (XRD) and low-temperature N_2-adsorption measurements. The adsorption characteristics of TiO_2 and supported gold particles are studied with the help of temperature-programmed desorption of O_2 (TPD-O_2). In order to compare our results with TiO_2 of normal morphology, parallel experiments were conducted on a Degussa P-25 photo-catalyst. *In situ* IR spectroscopy helped us in examining the surface species formed on NT and Au/NT samples as a result of room-temperature exposure to acetaldehyde in the presence of air. The reaction mechanism and the role of gold nanocrystallites in UV-mediated photo-catalytic oxidation of acetaldehyde are discussed on the bases of these investigations.

2. Experimental methods

The titania nanotubes were synthesized by utilizing a mesoporous TiO_2 sample as precursor, the preparation of which has been described elsewhere [14]. In brief, ~10 ml Ti(IV) isopropoxide (Aldrich) was added slowly to 1N HCl containing tartaric acid (3.6 g). The solution, stirred constantly for ~1 h, was heated for 24 h at 403 K in a teflon-lined autoclave. After cooling and centrifugation, the mass was dried (373 K) and calcined at 623 K for ~3 h. The TiO_2 nanotubes were obtained by a widely reported single alkali treatment procedure [16,17]. For this, 2 g of above-mentioned mesoporous TiO_2 was stirred with 10 M aqueous NaOH in a sealed polythene reactor maintained at a temperature of 393 K for 3 days. HCl solution was then added until the pH was ~1.5, followed by stirring for 24 h. After centrifugation, the precipitate was washed several times with water. The mass was finally freeze-dried (230 K) for 24 h prior to calcination for 3 h at different temperatures of 423 and 523 K, and these samples are denoted, respectively, as NT1 and NT2 (Table 1). About 1–1.5 wt.% of gold was incorporated in these two samples by impregnation with isopropanol solution of tetrachloroauric acid. After drying, the samples were heated again in air at their respective calcination temperature and are denoted as respective Au/NT samples in Table 1. A Degussa P-25 TiO_2 sample (denoted as T1) was employed as standard for some comparative studies.

The catalysts were characterized for their structural, optical and photo-catalytic properties. The powder XRD patterns were recorded on a Rigaku, Miniflex (D Max III VC) XRD machine (Cu Kα radiation), operated at 30 kV and 15 mA. The HRTEM images were obtained on Tecnai (model-F30) 300 kV field emission gun (FEG) transmission electron microscope, supplied by FEI Company (Netherlands). The information about the BET surface area and the pore characteristics of different samples was derived from the low-temperature nitrogen adsorption isotherms, recorded on a Quantachrome, NOVA 1200 equipment. Prior to recording of these data, the sample was treated at 573 K under vacuum (10^{-3} Torr) to remove the physisorbed moieties. The Barret–Joyner–Halenda (BJH) procedure was employed to obtain the pore size distribution data. The absorbance spectra were recorded on PerkinElmer (Lambda 650) UV–visible diffuse-reflectance spectrophotometer. About 3 wt.% of a sample was mixed thoroughly in barium sulphate for these measurements. XPS analyses were performed in an ultra-high vacuum system equipped with a VG Scientific ESCA-3000 spectrometer, operating at 150 W. The spectra were acquired using non-monochromatised Mg Kα radiation (1253.6 eV). The binding energy scale was calibrated taking adventitious C1 s line at 284.6 eV for charge compensation.

A Micromeritics Autochem 2910 instrument was employed for recording temperature-programmed desorption (TPD) profiles of oxygen adsorbed in the samples at saturation coverage. For each experiment, ~0.25 g of a fresh sample was placed in a U-shaped flow-through quartz microreactor. The sample was activated at 600 K for 3 h under He flow (20 ml min^{-1}) and then cooled to ambient temperature before exposure to O_2 (~20 vol% in He) flow for 30 min. The sample was flushed again in He for about 15 min to remove physisorbed oxygen, and desorption profile was then recorded by increasing the sample temperature to 1000 K at a ramp rate of 10 K/min. The activation energy (E_a) corresponding to different desorption peaks was determined by conducting TPD experiments at different heating rates (β) and following a method described elsewhere [18]. The value of E_a was estimated from the slope of a plot of $\ln(T_m^2/\beta)$ versus $1/T_m$, where T_m is the position of the peak maximum.

The photo-catalytic activity of the nanotube samples, without or with addition of gold, was monitored for oxidation of acetaldehyde under UV radiation (400 W medium-pressure mercury vapor lamp, Luminous flux—24,000 Lumens, photon flux—5×10^{19} photons s^{-1}, UV output 15–20%, range 225–400 nm, peak at 365 nm). The light source was housed in a water-cooled quartz jacket to cut-off infrared radiation. About 25 mg of a sample was placed in a quartz photo-reactor of 100 ml capacity and the acetaldehyde vapor mixed at different mol ratios (5–10 mol%) in air was introduced in the reactor for activity measurement. The experiments were conducted at room temperature and the reaction products formed as a function of radiation exposure were analyzed periodically with the help of a Nucon (Delhi, India) gas chromatograph (temperature-programmed Porapak-Q or molecular sieve column, TCD detector).

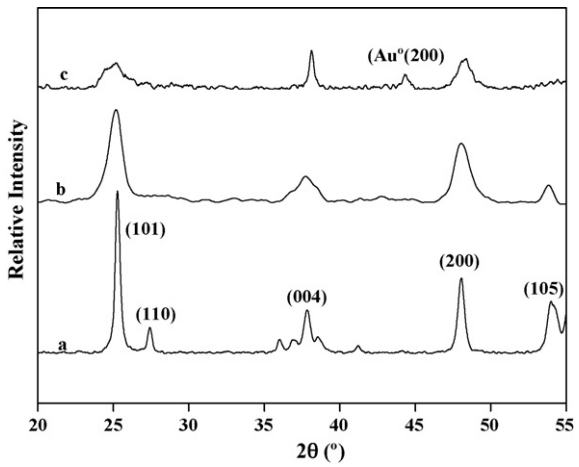

Fig. 1. Powder XRD patterns of TiO_2 nanotubes NT2 (curve b) and corresponding Au (1%)/NT2 sample (curve c). Curve (a) shows XRD reflections of Degussa P-25 TiO_2.

At the end of an experiment, the qualitative product analyses were also conducted by using a GC–MS (Shimadzu, model-R-15A) or alternatively an IR spectrophotometer (Shimadzu, model SSU-8000) equipped with a gas cell.

In situ FTIR experiments were conducted in the diffuse-reflectance (DR) mode to examine the surface species formed on adsorption of acetaldehyde over nanotube samples in the presence of oxygen. A Shimadzu SSU-8000 spectrophotometer was used for the DR study, and about 20 mg catalyst powder was packed in the sample holder for this purpose. The sample was cleaned by heating at 625 K for about 1 h followed by cooling to room temperature under nitrogen. Subsequently, about 10 ml mixture of acetaldehyde vapor (~15 mol%) + air was dosed over the sample kept under nitrogen flow (20 ml min^{-1}) and the IR spectra were recorded as a function of time. The sample spectrum recorded prior to acetaldehyde adsorption was compensated for plotting of the IR bands arising exclusively due to the surface adsorbed species. Acetaldehyde of extra-pure grade (99.5% purity, ACROS organics, USA) was utilized without any purification.

3. Results

3.1. Structural and textural features

Table 1 summarizes the surface area, pore dimensions and average crystallite size of different samples used in this study. Compared to P-25 TiO_2 (sample T1), nanotube samples exhibited significantly higher surface area and pore sizes. N_2-adsorption/desorption isotherms and the BJH pore size distribution plots demonstrated that the nanotubes samples were of mesoporous morphology, as shown in the results compiled in Table 1. The gold impregnated samples showed comparatively smaller surface area and pore openings, indicating the inclusion of some gold particles inside the tubular structures. Calcination at a lower temperature of 423 K resulted in smaller size crystallites and also in smaller pore openings due to the incomplete removal of template molecules. On the other hand, calcination at temperatures above 600 K led to some damage to the nanotube structure. Further details about the effect of calcination on the stability and the N_2-adsorption properties of TiO_2 nanotubes have been described earlier [19].

Curves b and c in Fig. 1 represent the XRD patterns of nanotube samples NT2 and Au (1%)/NT2, respectively. Corresponding XRD data for Degussa TiO_2 (T1) are presented in curve (a) in this figure. Sample T1 showed prominent XRD reflections at 2θ values of ca. 25.1°, 37.9°, 48° and 53.9°, representing (1 0 1), (0 0 4) (2 0 0) and (1 0 5) lattice planes of anatase TiO_2 (curve a). We also observe a weak reflection at $2\theta = 27.3°$ due to (1 1 0) plane of rutile phase, a characteristic of P-25 photo-catalyst. The XRD pattern in Fig. 1b thus demonstrates the presence of pure anatase crystal phase in the synthesized nanotubes. The broadening observed in the XRD pattern of NT2 (curve b) represents a quantum size effect in small (nano) size particles. Further broadening of XRD reflections in Fig. 1c and the changes observed in the relative intensity are indicative of the increased amorphous content in sample Au(1%)/NT2. This may be ascribed to the partial breakdown of the long range order in TiO_2 lattice and also some distortion in the tubular morphology of the nanotubes because of the occlusion of nanosize gold particles, as is revealed by the TEM and N_2-adsorption results of this study. The average size of crystallites in different samples, as estimated by using Scherrer's equation for I_{100} reflection at 25.1°, is listed in Table 1.

3.2. TEM results

Fig. 2a, b exhibit transmission electron microscopy (TEM) images of Au (1%)/NT1, showing a plane-view at two different magnifications. The low-magnification TEM image in Fig. 2a matches with the well reported picture of titania nanotubes comprising of multiple linear walls [16,17]. The tubular structures in Fig. 2a have average inner shell diameter of ca. 5.5 nm and the tube diameter varied from 8 to 13 nm with an average of about 10.0 nm. The length of the tubes varied in a wide range of 0.1–0.3 μm and most of them are seen to be open at both the ends. The coating along some selective nanotubes and the dark round shape spots of high scattering contrast arise from the gold crystallites, distributed randomly both within and at the external surfaces of TiO_2 nanotubes in Fig. 2a. TEM pictures obtained at a higher resolution further revealed that the gold crystallites seen in Fig. 2a are in fact agglomerates of the smaller size gold particles. Fig. 2b exhibits a representative high-resolution TEM picture of the gold-coated area of a nanotube. This micrograph clearly shows the presence of almost uniform size (1.5–5 nm) gold particles (marked with arrows). In the high-resolution lattice images of one of the dark spots in Fig. 2a, the fringes exhibited a d-spacing of 2.03 Å in match with the (2 0 0) plane of gold metal.

The selected area electron diffraction (SAED) pattern in Fig. 2c, taken from a single nanotube, illustrates two innermost rings with average d-spacing of around 3 and 1.6 Å. These correspond to (1 1 0) and (2 2 0) lattice planes of anatase TiO_2. Also, these diffraction rings show characteristic features of amorphous materials, in conformity with our XRD results (Fig. 1). The bright spots within these rings show the d-spacing of 2.03 Å, corresponding to the (2 0 0) plane of gold metal.

The TEM micrographs of the high temperature calcined samples, i.e. Au(1%)/NT2 and Au(1.5%)/NT2, exhibited similar features, besides some areas of amorphous nature and also the presence of some larger size gold clusters. Picture (d) in Fig. 2 exhibits a representative TEM image of Au (1.5%)/NT2 sample, where such large crystallites of gold (10–70 nm size) are seen clearly. Fig. 2d also shows the breakdown of the tubular structure in certain areas, as mentioned above.

3.3. Absorbance measurements

Fig. 3 presents the diffuse-reflectance UV–visible spectra of nanotube samples NT1 (curve a), NT2 (curve b) and corresponding gold composites, i.e. Au(1%)/NT1 (curve c) and Au(1%)/NT2 (curve d). Curve (e) in this figure shows a spectrum of sample T1 for comparison. A decrease in absorbance is noticed for nanotubes of TiO_2 in the wavelength range of 200–400 nm (curves b), as compared to Degussa TiO_2 (curve e). Also, the spectral intensity

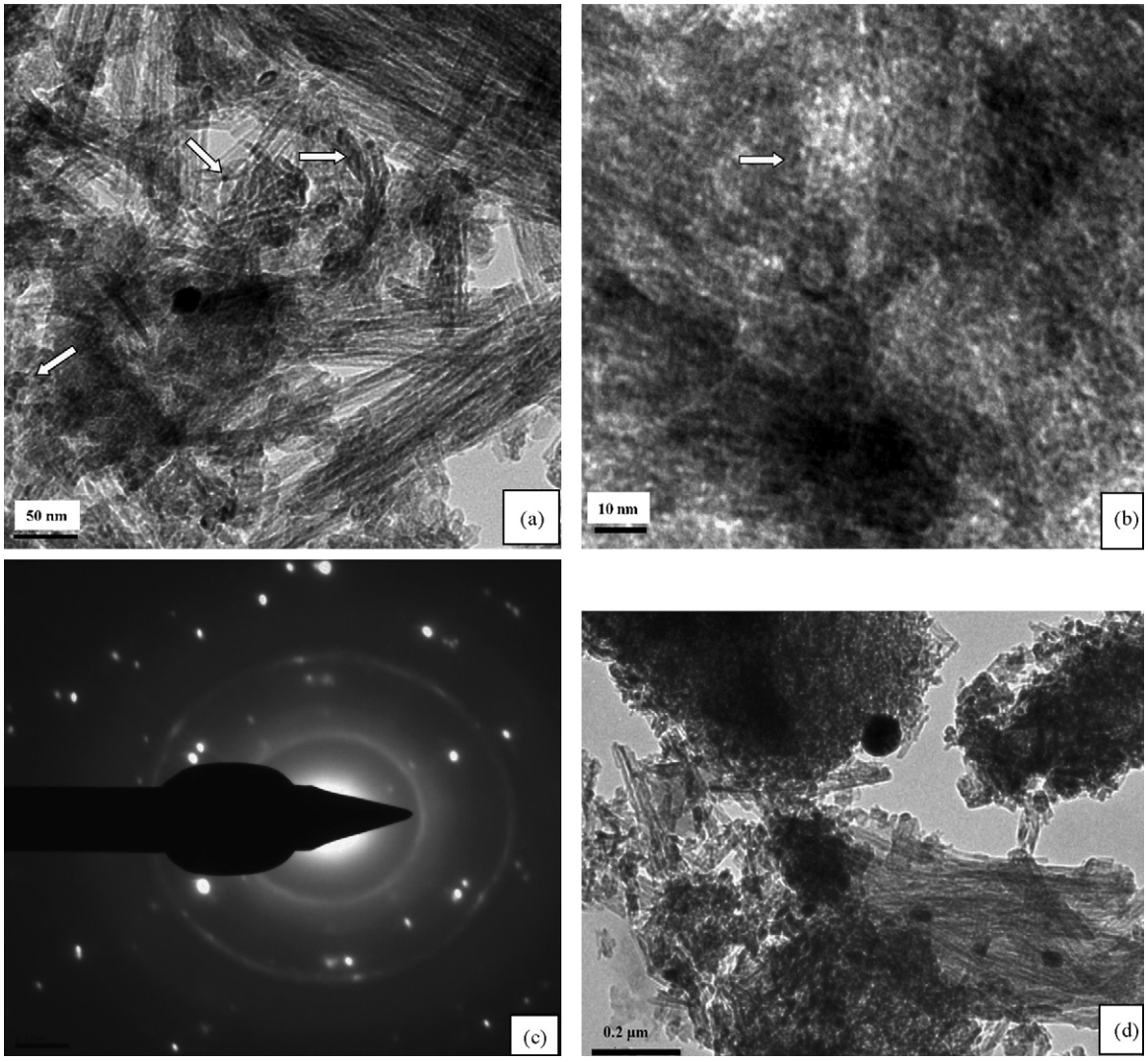

Fig. 2. TEM of Au (1 wt.%)/TiO_2 nanotubes (NT1): pictures (a) and (b) show the micrographs at two different magnifications while image (c) presents a selected area electron diffraction pattern. (d) TEM picture of a higher temperature calcined sample Au (1.5 wt.%)/NT2.

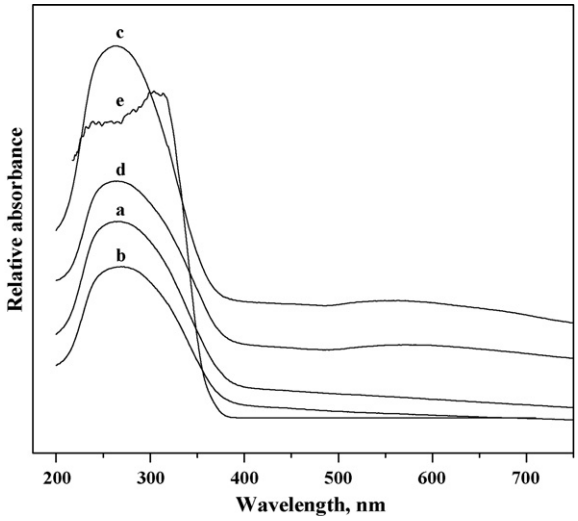

Fig. 3. Diffuse-reflectance UV–visible spectra of different TiO_2 and Au/TiO_2 nanotube samples: Curve (a) NT1, (b) NT2, (c) Au(1%)/NT1, (d) Au(1%)/NT2. Curve (e) presents similar data for sample T1.

decreased further on calcination of the as-synthesized nanotubes at an elevated temperature (curve b). The incorporation of gold, on the other hand, resulted in considerable increase of absorbance, both in UV and in visible regions (curves c, d). In addition to these intensity changes, a shift to lower wavelength is also noticeable in the UV–visible spectra of nanotube samples (curves a–d), a feature characteristic of nano-structured materials. A broad and weak absorbance band in 500–600 nm range, as seen in curves c and d of Fig. 3, is due to well reported plasmon resonance phenomenon associated with nano-structured gold particles [20].

3.4. XPS analysis

Curve (b) in Fig. 4 presents Au4f XPS spectrum of gold dispersed titania nanotubes (Au1%/NT2). Comparative spectrum of pure gold powder, prepared by reduction of a chloroauric acid solution, is shown in Fig. 4a. The binding energy (B.E.) values of 84.2 and 87.8 eV for $4f_{7/2}$ and $4f_{5/2}$ electrons in Fig. 4b match well with the values for small zerovalent gold particles and also with the corresponding data recorded for a pure gold powder (Fig. 4a). Our XPS data thus rule out any metal–support interactions or the presence of ionic gold in our samples.

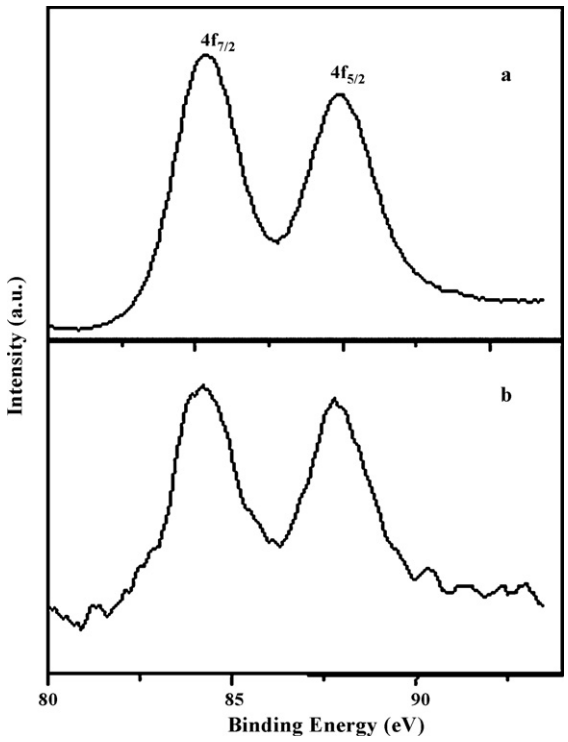

Fig. 4. 4f XPS spectra of gold. Curve (a) pure gold metal, (b) gold-coated nanotube sample Au(1%)/NT2.

3.5. TPD-O_2 results

The temperature-programmed desorption profiles of O_2 adsorbed over P-25 TiO_2 and the nanotube sample NT1 revealed that the adsorption states of O_2 are influenced considerably by the morphology/texture of a TiO_2 sample. Thus, the non-porous sample T1 gave rise to a broad and tailing desorption band with temperature maximum (T_m) at ~620 K (Fig. 5, curve a). On the other hand, the desorption profile of NT1 exhibited at least three distinct overlapping bands at 635, 760 and 870 K, indicating the adsorption/entrapment of oxygen molecules at different sites with corresponding activation energy (E_a) of ca. 30.0, 36.0 and 41.5 kcal mol^{-1}. Curve (b) in Fig. 5 presents a typical O_2 desorption profile of nanotubes NT1. On comparing the curves (a) and (b) and in consideration of the E_a values, the 620 K band may be attributed to the O_2 molecules adsorbed at external surface and the higher temperature bands in Fig. 5b to the molecules trapped in the narrow tubular structures of NT1. The intensity of the high temperature desorption bands was found to decrease significantly when a second run of desorption pattern was recorded on the residual sample of Fig. 5b, after exposing it *in situ* at room temperature to O_2 flow and then flushing under helium. This confirmed our assignment of 760 and 870 K TPD peaks to the encapsulation of O_2 molecules in the pores of the nanotubes.

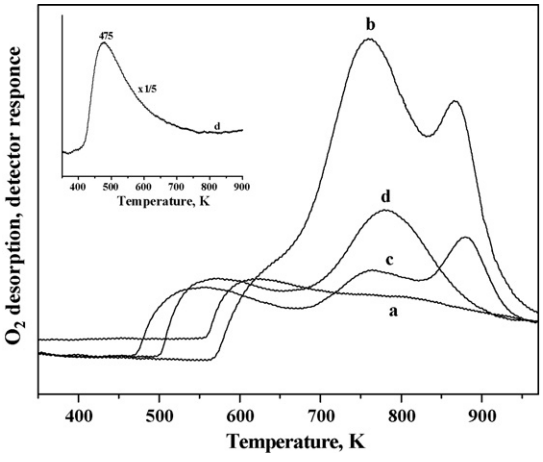

Fig. 5. Comparative temperature-programmed desorption profile of O_2 from TiO_2 nanotubes and their gold composites. Curve (b) nanotubes NT1, (c) Au (1%)/NT1, (d) Au (1%)/NT2. Curve (a) presents corresponding TPD-O_2 profile of Degussa TiO_2. Curve d (inset) shows a second cycle O_2 TPD profile of Au (1%)/NT1.

The presence of gold resulted in considerable decrease in the intensity of high temperature TPD bands mentioned above, and at the same time a new low-temperature desorption band was observed at ~550 K (E_a ~ 26.4 kcal mol^{-1}). The typical TPD-O_2 profile of sample Au (1%)/NT1 is shown in Fig. 5c. The TPD-O_2 profile of Au (1%)/NT2, subjected to calcination at an elevated temperature of 523 K, is shown in Fig. 5d. The absence of 870 K peak in Fig. 5d (cf. Fig. 5b) may be attributed to the blockage of pores by gold particles and possibly some damage to the tubular structures, as is evident from the TEM image in Fig. 2d. This is in agreement with our N_2-adsorption results described above (Table 1). The new desorption band at 550 K in Figs. 5 c, d can be identified with the adsorption of O_2 at Au–TiO_2 interfacial sites. As in the case of O_2 entrapment in titania nanotubes, no O_2-adsorption was observed over gold particles after calcination of Au/NT samples. For instance, curve (e) in the inset of Fig. 5 exhibits a typical second cycle O_2 TPD profile of Au(1%)/NT2. Our TPD results thus clearly reveal that the gold particles give rise to certain new adsorption sites at Au–TiO_2 interfaces that facilitate the adsorption and the activation of O_2 molecules. Furthermore, our results also confirm that the adsorption characteristics of Au are very sensitive to particle size (Fig. 5e).

3.6. Photo-catalytic activity

All the samples under this study gave rise to formation of CO_2 as a major reaction product during the gas-phase room-temperature oxidation of acetaldehyde under UV-irradiation. In addition, formation of small amounts of hydrogen, methane, carbon monoxide and also an unidentified product were detected by GC analysis. No reaction occurred without irradiation. The yield of these reaction products, however, depended considerably upon the textural properties of TiO_2 photo-catalyst as well as the presence of Au co-catalyst. These results are presented in Figs. 6 and 7. Fig. 6 displays the yield of CO_2 when acetaldehyde (8 mol%) + air were reacted under ultraviolet irradiation over Degussa sample T1 (curve b), nanotubes NT2 (curve c), and the gold-containing samples Au(1%)/NT2 and Au(1.5%)/NT2 (curves d, e). As seen in these results, higher yields of CO_2 were obtained using TiO_2 nanotubes compared to sample T1, as commensurate to the higher surface area of NT2 (Table 1). Furthermore, an appreciably higher conversion of acetaldehyde was observed in case of the gold-containing samples, the yield of CO_2 increasing with gold content (Fig. 6d, e). Not only the increase in CO_2 yields, the saturation yields were attained faster in the case of gold-containing samples (Fig. 6d, e). This may be attributed to the presence of some gold-induced additional adsorption sites in Au/NT samples, as discussed later in detail.

It needs a mention that the oxidation of acetaldehyde was observed under UV-irradiation even in the absence of a catalyst, albeit with much smaller product yields. These comparative data are shown by curve (a) in Fig. 6.

Similar trends were noticed in the yield of other reaction products, viz. CH_4 and H_2, the gold-containing samples giving rise to much higher conversion as compared to T1, and also the gold-free nanotube samples. These results, obtained on representative samples NT2 and Au(1%)/NT2, are illustrated in Fig. 7. The mass spectral analysis showed that in addition to the reaction products

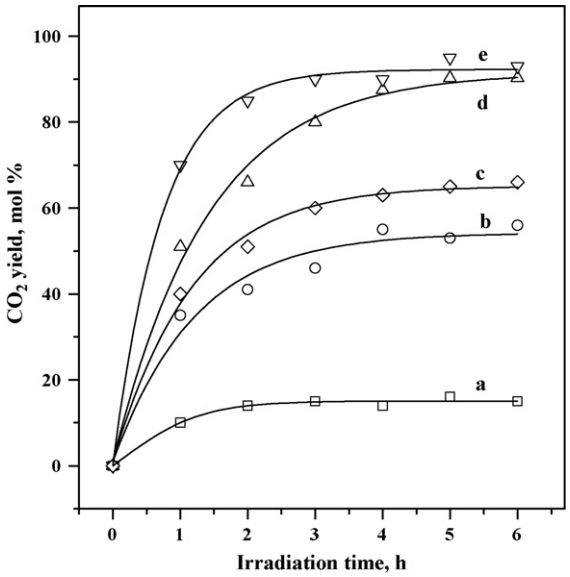

Fig. 6. Plots of CO_2 yield when acetaldehyde (8 mol%) + air were reacted at room temperature over Degussa and nanotube TiO_2 samples under irradiation. Curve (b) T1, (c) NT2, (d) Au(1%)/NT2 and (e) Au(1.5%)/NT2. Curve (a) shows radiation induced conversion of acetaldehyde to CO_2 without using any catalyst.

mentioned above, small amounts of water (m/e = 18), iso-propanol (m/e = 45) and acetic acid (m/e = 60) were also formed. The yields were however non reproducible and no attempt was made to make a quantitative estimation of these minor products. We may also mention that the rate of acetaldehyde oxidation also depended upon its concentration in the air, the reaction rate being faster for smaller CH_3CHO: air mol ratios in the reaction mixture, as has also been reported in our earlier study on acetone oxidation [14].

3.7. Infrared spectroscopy of surface adsorbed species

Curve b in Fig. 8 presents the difference IR spectrum showing the surface species formed over titania nanotubes (NT2) within ~1 min of room-temperature exposure to a dose (~10 ml) of CH_3CHO + air under nitrogen flow. Curve (a) shows a comparative infrared spectrum of acetaldehyde mixed in air. The IR spectra recorded after the post-exposure delay time of 3 and 15 min are shown in curves

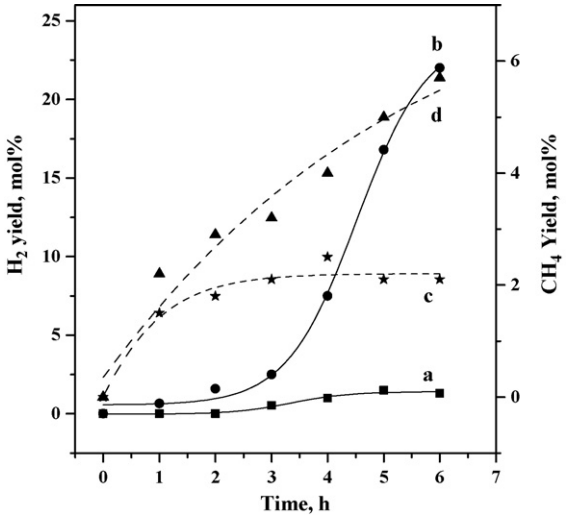

Fig. 7. Yield of H_2 (curves a, b) and CH_4 (curves c, d) as a function of irradiation time when acetaldehyde (8 mol%) + air were reacted at room temperature over samples NT2 (curves a, c) and Au(1%)/NT2 (b, d).

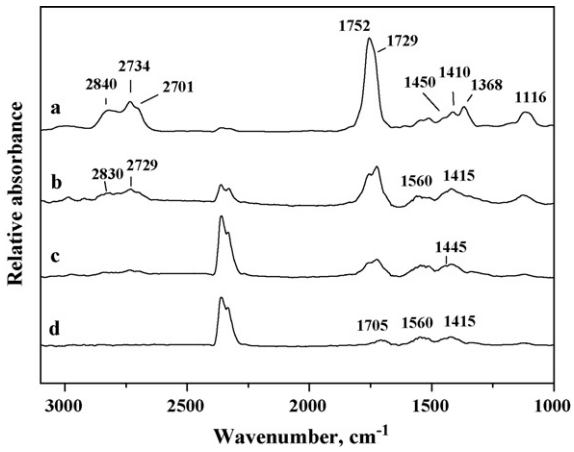

Fig. 8. Difference IR spectra showing surface species formed over titania nanotubes (NT2) on exposure to acetaldehyde (15 mol%) + air at room temperature followed by flushing under nitrogen flow for (b) 1 min, (c) 3 min, and (d) 15 min. Curve (a) shows corresponding IR spectrum of acetaldehyde + air.

(c) and (d), respectively, of Fig. 8. A comparison of IR spectra in Fig. 8a and b reveal a considerable change in the relative intensity and the peak widths of the vibrational bands of acetaldehyde, e.g. 2840–2700 cm^{-1} region bands due to C–H stretch bands of α-carbon, 1368 cm^{-1} band due to umbrella bending of methyl groups, 1410 cm^{-1} band arising due to asymmetric bending mode vibrations of the methyl group, and also the 1116 cm^{-1} band due to $\gamma(CH_3)$ and ν(C–C) vibrations of acetaldehyde. These changes arise from the molecular adsorption of acetaldehyde over metal oxides, including titania [21]. The adsorbed acetaldehyde transformed quickly to form some broad and overlapping bands with their frequency maxima at around 1560, 1470, 1445, and 1340 cm^{-1} (Fig. 8c, d). These bands may be identified with the adsorbed acetate ($CH_3COO^-{}_{ad}$) species (ν_{as}(COO) 1560, $\delta_{as}(CH_3)$ 1470, δ_s(COO) 1445, $\delta_s(CH_3)$ 1340 cm^{-1}), as reported in several previous publications [21,22]. The presence of a carbonyl band at ~1705 cm^{-1} (Fig. 8d) indicates the presence of carbonyl containing adsorbed species. Even though it is difficult to predict the identity of the molecules that may give rise to such IR bands, the overlapping broad bands in Fig. 8c, d indicate the presence of more than one kind of surface adsorbed species. The presence of adsorbed formate ($HCOO^-{}_{ad}$) species is one such possibility, where the IR bands are known to appear at 2846 cm^{-1} (νCH), 1580 cm^{-1} (ν_{as}COO), 1416 cm^{-1} (δCH), and 1350 cm^{-1} (ν_sCOO) [22]. The formation of adsorbed CO_2 (ν(COO) IR bands at 2360 and 2329 cm^{-1}) is also observed in Fig. 8c, d, which may have its origin in the decomposition of some of the above-mentioned transient species.

The spectral features described above were accompanied with the simultaneous removal of various hydroxyl region stretching bands of adsorbent TiO_2, i.e. 3700, 3670 and 3610 cm^{-1}, as shown by the negative bands in IR spectra. The relative intensities of these bands varied as a function of time. These results are presented in curve (a) and (b) of Fig. 9, recorded after the delay time of 1 and 15 min, respectively, after the exposure of NT2 to acetaldehyde. It is likely that the instant removal of the OH bands after adsorption of acetaldehyde (Fig. 9a) is offset by the regeneration of these species over TiO_2 surface by the water molecules produced during reaction (Fig. 9b).

It is important to place on record that similar IR results were obtained in the experiments conducted on other samples, including Au/NT, barring some changes in the relative intensity of the IR bands. This indicates that the basic steps involved in the interaction of acetaldehyde over TiO_2 may by and large remain unaffected by the presence of gold particles.

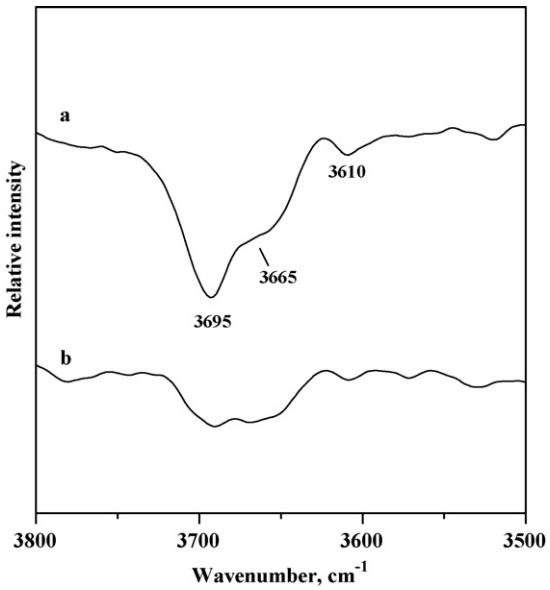

Fig. 9. Hydroxyl region IR spectra of titania nanotubes (NT2) after room-temperature adsorption of acetaldehyde + air under N_2 flow and recorded after different delay times. Curve (a) 1 min and curve (b) 15 min.

4. Discussion

Several studies have been reported previously on TiO_2-mediated photo-catalytic oxidation of acetaldehyde [23–27]. As mentioned in introduction, different views have been expressed in regards to the effect of particle size on the photo-catalytic properties of metal supported titania. In a study by Xu et al. [26], the enhanced photoactivity of titania nanotubes compared to that of standard P25 is attributed to the surface charge polarity developed on outer and inner surfaces that in turn helps in enhancing the electron–hole pair separation. The promotional effect of doped Au or Pt is found to depend on particle size, the activity decreasing with increase in crystallite size. In a recent publication from Anpo's group [27], the high activity of TiO_2/ZSM-5 for photooxidation of acetaldehyde is found to be related to the hydrophobicity of the zeolite support. As discussed in a recent review [28], the unusual catalytic properties of TiO_2-gold composite nanoparticles have often been attributed to the transfer of electrons from excited TiO_2 into Au, leading thereby to their equilibration and resultant better separation of the charges. No concerted efforts have, however, been made so far to explore a possible relationship between the photo-catalytic activity and the morphology-dependent adsorptive properties of a semiconductor.

The present study provides some new insights on various unresolved issues, as discussed above. Following are the highlights:

(i) IR results show that the acetaldehyde molecules bind weakly over titania surface (Fig. 8b), and oxidize quickly to form certain acetate and formate type ad-species under ambient conditions (Fig. 8c, d). The simultaneous removal of surface hydroxyl groups and their subsequent regeneration (Fig. 9a, b) demonstrate the involvement of hydroxyl groups or adsorbed water molecules in this process, as has been reported in earlier studies as well. The gold particles, on the other hand, may play a negligible role in this initial step of the photoreaction.

(ii) Activity results in Fig. 6a reveal that the photo-oxidation of acetaldehyde may occur, though to a small extent, even in the absence of TiO_2. It is thus evident that the primary step involved in acetaldehyde degradation is a free-radical or ion-radical formation, a process that may initiate either on direct photo-irradiation or with the help of UV-mediated e^-/h^+ pairs in TiO_2, depending upon the nature of a reacting organic molecule. Subsequent recombination and transformations of the transient species thus formed may occur on the reactor walls as well as in an adsorbed state over the titania surface. The activity trend observed in plots a–c in Fig. 6, viz. NT > Degussa > no catalyst, follows a trend similar to that of the surface areas of these samples (Table 1). We can therefore conclude that the morphology and the surface characteristics of a photo-catalyst may play an important role in these photochemical processes.

(iii) We observe that in spite of being in pure anatase phase (Fig. 1) and also in spite of a shift to lower wavelength in absorption band (Fig. 3), TiO_2 nanotubes display higher catalytic activity compared to a Degussa P25 photo-catalyst (Fig. 6b). A similar relationship is observed between the amount of oxygen adsorbed/entrapped and the catalytical activity of other samples as well (Figs. 6 and 7). Our results thus confirm that besides the interfacial charge separation processes, the morphology-dependent augmentation in the adsorption at reaction sites may control the overall quantum efficiency of a photo-catalyst.

(iv) Our TPD results reveal that the nanosize particles of gold give rise to distinct low-energy sites for the adsorption of O_2 molecules (Fig. 5 curves c, d). The unique catalytic properties of gold–metal oxide interfaces for the adsorption and activation of oxygen molecules have been amply demonstrated in earlier studies [29–31]. In these studies, the nano-dispersed gold particles are shown to exhibit extra-ordinary properties, similar to that of Pt, where the adsorbed O_2 molecules get activated/dissociated to form the surface bonded Au-$O^\bullet$ species. Also, the ESR and O_2 TPD studies on a TiO_2 supported gold catalyst have demonstrated that O_2 molecules adsorbed at Au/TiO_2 interfaces may transform to superoxide, i.e. O_2^- ion radicals [31]. As is well known, the O_2^- species may also form on electron scavenging by oxygen molecules at the surface of the photo-excited Au/TiO_2. Similarly, the oxidation of water on photo-activated catalyst is known to generate hydroxyl ion radicals [32]. Ultimately, the decomposition and oxidation of acetate or formate surface species with the help of the ion radicals or free radicals thus formed on photoexcitation of TiO_2 would give rise to the reaction products obtained in this study.

The possible reaction pathways assisted by such free- or ionic radicals have been discussed and reviewed in a large number of articles [5,26,32–35]. Among the various possible mechanisms, the UV-mediated oxidation of acetaldehyde may involve the following reaction steps.

$$TiO_2 + h\nu \rightarrow e^- + h^+$$

$$O_2 + e^- \rightarrow {O_2}^-{}_{ad}$$

$$H_2O_{ad} + h\nu \rightarrow H^+ + OH^-$$

$$Au + O_2 \rightarrow Au\text{–}O_{2ad} \rightarrow Au\text{–}O_{ad}$$

$${OH^-}_{ad} + h^+ \rightarrow {}^\bullet OH$$

$$H^+ + e^- \rightarrow H_{ad}$$

$$CH_3CHO_{ad} + OH(TiO_2) \rightarrow HCOOCH_{3ad} + H_{ad}$$

$$CH_3CHO_{ad} + OH(TiO_2) \rightarrow HCOOH_{ad} + {}^\bullet CH_{3ad}$$

$$HCOOCH_{3ad} + e^- \rightarrow {}^\bullet CH_3 + {HCOO^-}_{ad}$$

$CH_3CHO_{ad} + {O_2}^-{}_{ad} \rightarrow OH_{ad} + CH_3COO^-{}_{ad}$

$CH_3COO^-{}_{ad} + h^+ \rightarrow {}^\bullet CH_3 + CO_2$

$CH_3CHO + O_{ad}(Au) \rightarrow CO_2 + CH_4$

$HCOO^-{}_{ad} + h^+/OH \rightarrow CO_2 + H_2O$

$HCOO_{ad} + O_{ad}(Au) \rightarrow CO_2 + OH_{ad}$

$CH_3CHO + O_{ad}(Au) \rightarrow CH_3COOH$

${}^\bullet CH_3 + {}^\bullet CH_3 \rightarrow C_2H_6$

${}^\bullet CH_3 + H_{ad} \rightarrow CH_4$

$H_{ad} + H_{ad} \rightarrow H_2$

5. Conclusion

Detailed physico-chemical and photo-catalytic properties of titania nanotubes and corresponding gold-containing samples are investigated in detail, using UV-mediated oxidation of acetaldehyde as a probe reaction. The highly dispersed gold and Au^0–TiO_2 interfaces are found to serve as distinct low-energy sites for the direct adsorption and activation of O_2 molecules. On the other hand, the tubular structure of TiO_2 facilitated the entrapment of oxygen, requiring a high temperature (>650 K) for subsequent thermal desorption. The overall photo-catalytic process involves the generation of acetate or formate type surface transient species during the interaction of acetaldehyde + O_2 over TiO_2 in presence of hydroxyl groups, followed by the reactions with charge pair mediated free radicals (e.g. $OH^\bullet$) or ionic radicals (e.g. O^{2-}, O^-) at Au/TiO_2 interfaces. Based on different physico-chemical, structural and optical properties of the samples employed in this study, we conclude that besides e^-/h^+ charge separation the adsorptive properties associated with the host TiO_2 semiconductor and the dispersed nanosize gold particles may play a significant role in the overall photo-catalytic processes.

Acknowledgements

N.M. Gupta thanks the CSIR for an ES Research Grant. Ms. V. Samuel and Mr. R.K. Jha are thanked for XRD and N_2-adsorption measurements. Our thanks are also due to Dr. Shubhangi B. Umbarkar and Ms. Trupti for their help in recording the IR data. M/s Degussa India Pvt. Ltd., Mumbai are thanked for the gift of a P25 TiO_2 sample.

References

[1] D. Beydoun, R. Amal, G. Low, S. Mc Evoy, J. Nanoparticle Res. 1 (1999) 439.
[2] B. Levy, J. Electroceram. 1 (1997) 239.
[3] Y. Wang, N. Herron, J. Phys. Chem. 95 (1991) 525.
[4] A.L. Linsebigler, G. Lu, J.T. Yates Jr., Chem. Rev. 95 (1995) 735.
[5] M.R. Hoffman, S.T. Martin, W. Choi, D.W. Bahnemann, Chem. Rev. 95 (1995) 69.
[6] N. Serpone, D. Lawless, R. Khairutdinov, E. Pellizzetti, J. Phys. Chem. 99 (1995) 16655.
[7] Z. Zhang, C.-C. Wang, R. Zakaria, J.Y. Ying, J. Phys. Chem. B 102 (1998) 10871.
[8] A.J. Hoffman, G. Mills, H. Yee, M.R. Hoffmann, J. Phys. Chem. 96 (1992) 5546.
[9] R.F. Khairutdinov, Russ. Chem. Rev. 67 (1998) 409.
[10] V. Subramanian, E. Wolf, P.V. Kamat, J. Phys. Chem. B 105 (2001) 11446.
[11] C.-G. Wu, C.-C. Chao, F.-T. Kuo, Catal. Today 97 (2004) 109.
[12] Y. Sakatani, D. Grosso, L. Nicole, C. Boissière, G.J. de, A.A. Soler-Illia, C. Sanchez, J. Mater. Chem. 16 (2006) 77.
[13] M.-J. Lopez-Munoz, R. van Grieken, J. Aguado, J. Marugan, Catal. Today 101 (2005) 307.
[14] S.V. Awate, A.A. Belhekar, S.V. Bhagwat, R. Kumar, N.M. Gupta, Int. J. Photoenergy 2008 (2008) 1–13, Article ID 789149.
[15] P.S. Lunawat, R. Kumar, N.M. Gupta, Catal. Lett. 121 (2008) 226.
[16] Q. Chen, W. Zhou, G. Du, L.-M. Peng, Adv. Mater. 14 (2002) 1208.
[17] R. Yoshida, Y. Suzuki, S. Yoshikawa, Mater. Chem. Phys. 91 (2005) 409.
[18] P.T. Dawson, P.C. Walker, in: R.B. Anderson, P.T. Dawson (Eds.), Experimental Methods in Catalytic Research, vol. III, Academic Press, New York, 1976, p. 211.
[19] S.V. Awate, R.K. Sahoo, M.D. Kadgaonkar, R. Kumar, N.M. Gupta, Catal. Today 141 (2009) 144.
[20] C.-M. Yang, M. Kalwei, F. Schuth, K.J. Chao, Appl. Catal. A 254 (2003) 289.
[21] J. Rasko, J. Kiss, Appl. Catal. A 287 (2005) 252.
[22] Z. Yu, S.S.C. Chuang, J. Catal. 246 (2007) 118.
[23] C. Shifu, C. Xueli, T. Yaowu, Z. Mengyue, J. Chem. Technol. Biotechnol. 73 (1998) 264.
[24] J.L. Falconer, K.A. Magrini-Bair, J. Catal. 179 (1998) 171.
[25] J. Wang, S. Uma, K.J. Klabunde, Appl. Catal. B 48 (2004) 151.
[26] H. Xu, G. Vanamu, Z. Nie, H. Konishi, R. Yeredla, J. Phillips, Y. Wang, J. Nanomaterials (2006) 1–8, Article ID 78902.
[27] M. Takeuchi, T. Kimura, M. Hidaka, D. Rakhmawaty, M. Anpo, J. Catal. 246 (2007) 235.
[28] P.V. Kamat, J. Phys. Chem. C 111 (2007) 2834.
[29] M. Haruta, Catal. Today 36 (1997) 153.
[30] S.H. Overbury, V. Schwartz, D.R. Mullins, W. Yan, S. Dai, J. Catal. 241 (2006) 56.
[31] H. Liu, A.I. Kozlov, A.P. Kazlov, T. Shido, K. Asakura, Y. Iwasava, J. Catal. 185 (1999) 252.
[32] R. Gao, J. Stark, D.W. Bahnemann, J. Rabani, J. Photochem. Photobiol. A 148 (2002) 387.
[33] V. Augugliaro, S. Coluccia, V. Loddo, L. Marchesc, G. Martra, L. Palmisano, M. Schiavello, Appl. Catal. B 20 (1999) 15.
[34] K. Bhattacharya, S. Varma, D. Kumar, A.K. Tripathi, N.M. Gupta, J. Nanosci. Nanotechnol. 5 (2005) 797.
[35] U. Siemon, D. Bahnemann, J.J. Testa, D. Rodriguez, M.I. Litter, N. Bruno, J. Photochem. Photobiol. A 148 (2002) 247.